## PAPER

# Effect of IR laser on myoblasts: a proteomic study

Monica Monici,[a] Francesca Cialdai,[a] Francesco Ranaldi,[b] Paolo Paoli,[b] Francesca Boscaro,[c] Gloriano Moneti[c] and Anna Caselli†[b]

Laser therapy is used in physical medicine and rehabilitation to accelerate muscle recovery and in sports medicine to prevent damages produced by metabolic disturbances and inflammatory reactions after heavy exercise. The aim of this research was to get insight into possible benefits deriving from the application of an advanced IR laser system to counteract deficits of muscle energy metabolism and stimulate the recovery of hypotrophic tissue. We studied the effect of IR laser treatment on proliferation, differentiation, cytoskeleton organization and global protein expression in C2C12 myoblasts. We found that laser treatment induced a decrease in the cell proliferation rate without affecting cell viability, while leading to cytoskeletal rearrangement and expression of the early differentiation marker MyoD. The differential proteome analysis revealed the up-regulation and/or modulation of many proteins known to be involved in cell cycle regulation, cytoskeleton organization and differentiation.

## Introduction

Since the seventies laser therapy has been widely used in sports medicine, physiatry and rehabilitation to treat muscle diseases of different origins: myalgias, contusions, sprains, lacerations and damage due to heavy exercise.[1–3] These diseases have in common the painful symptomatology, the inflammatory component and, in the case of injuries, the need to repair the tissue portion in which the muscle fibers have suffered damage. The application of laser therapy, either alone or combined with other treatments, both pharmacological and instrumental, has its rationale in the therapeutic effects that are attributed to laser radiation: analgesic, anti-inflammatory, anti-oedema and ability to promote wound healing and tissue repair. A large amount of literature shows that laser radiation can affect the cell energy metabolism and ATP production,[4,5] the response of immune cells to injury,[6] the production of inflammation mediators,[7–9] the behavior of fibroblasts[10–12] and endothelial cells.[13,14] Moreover, laser radiation can improve microcirculation[15] and relieve pain both indirectly through the effects mentioned above, and directly, by acting on receptors and nerve endings.[16–19]

Although many clinical studies give evidence for the effectiveness of IR laser therapy in the treatment of muscular disorders,

thus justifying the wide application of laser treatments in clinical rehabilitation and sports medicine, in the literature there are conflicting results[1,20–27] most likely caused by differences in the laser sources and treatment parameters that have been used.

In the last few years significant progress has been made in understanding the mechanisms by which the IR laser therapy promotes the healing process and recovery of muscle tissue. Recent studies, carried out both in animal models and human subjects, demonstrated that pre-exercise treatment with IR laser can significantly delay muscle fatigue and accelerate post-exercise recovery.[3,28] In rats, it has been found that laser treatment reduces the inflammatory response caused by experimentally induced muscle trauma and is able to block the effects of reactive oxygen species (ROS) release and the activation of NF-kB.[29] Laser-induced changes in inflammatory biomarkers and significant muscle recovery have been observed also in a rat model of myopathy.[30] Other authors found that, in traumatized muscle tissues, laser therapy induces an increase in activity of the complexes I, II, III and VI of the respiratory chain that may lead to an increase in ATP synthesis and faster muscle recovery.[5] A study aimed at evaluating the effectiveness of IR laser radiation in promoting the recovery of atrophied skeletal muscles demonstrated that the laser treatment favours tissue repair through activation of satellite cells and induction of neoangiogenesis.[31]

However, despite the fact that over the past decade numerous studies have significantly improved our knowledge, in many respects the effects of radiation emitted by different laser sources on muscle tissue and its repair mechanisms are far to be completely understood.

[a] *ASAcampus Joint Laboratory, ASA Res. Div., Dept. Clinical Physiopathology, University of Florence, Italy*
[b] *Dept. of Biochemical Sciences, University of Florence, Italy*
[c] *CISM Mass Spectrometry Center, University of Florence, Italy*
† *Dept. Biochemical Sciences, University of Florence, Viale Morgagni, 50, 50134 Florence, Italy. E-mail: anna.caselli@unifi.it; Tel: + 39 055 4598344.*
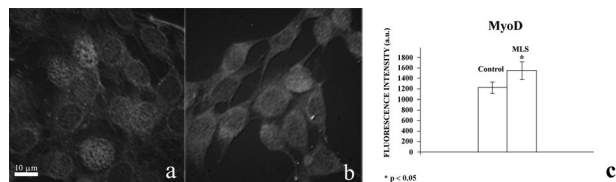
**Fig. 1** MyoD expression in C2C12 cells after MLS laser treatment. a: control C2C12 cells. b: MLS treated C2C12 cells. c: quantitative expression of MyoD. Images obtained by immunofluorescence microscopy show that, in cells treated with MLS laser, MyoD expression increased and the transcription factor was mainly distributed in the nuclear and perinuclear area. Image analysis revealed that in treated cells MyoD increased by about 26%, in comparison with controls.

This paper reports the results of a study aimed to investigate the behavior of C2C12 cells exposed to the emission of a dual wavelength IR laser. The C2C12 skeletal muscle cell line has been derived from murine satellite cells and is widely accepted as a model to study the behavior of satellite cells,[32] which play a crucial role in skeletal muscle regeneration and repair[33] and are capable of repopulating damaged and atrophied muscle.[34] The source chosen to perform the treatments was a synchronized IR dual emission laser system, with wavelengths of 808 and 905 nm, respectively. Most of the recent studies reported the effectiveness of laser emissions in the range 800–830 nm as well as emissions around 905 nm in triggering a biological response in muscle tissue. Sources with multiple emissions are widely used in clinics but little is studied from the point of view of the effects that induce in the cellular component of muscle tissue. We considered interesting to study the effects of a source that simultaneously emits two wavelengths which, on the basis of the literature, both can favour the recovery of homeostasis in diseased muscles.

The behavior of C2C12 cells was assessed before and after exposure to laser treatments in terms of cell viability, morphology, proliferation, differentiation and proteomic profile. To the best of our knowledge this is the first time that the effect of IR laser radiation on the proteomic profile of myoblasts is being studied.

## Results and discussion

### Effect of MLS laser treatment on viability, proliferation and differentiation of C2C12 cells

Murine myoblasts C2C12 were treated with a Multiwave Locked System laser (MLS laser) as described in the experimental section. Before proceeding to the appropriate morphological and proteomic studies, we analyzed the effect of the laser treatment on cell viability and proliferation. The trypan blue assay, performed both after a single exposure to the laser radiation and after 3 exposures carried out on consecutive days, showed that in treated samples there were no significant changes in cell viability (over 98%) compared to the control. The cell count did not show significant differences after a single exposure, whereas after 3 treatments with MLS laser, the cell number decreased moderately (about 23.4%) with respect to the control. Since MLS laser treatment does not

affect cell viability, we hypothesized that the reduced proliferation rate of MLS laser treated cells was caused by the triggering of a differentiative process. To verify our hypothesis we analyzed expression and distribution of MyoD, which is widely recognized as an early marker of myoblast differentiation. In fact it is known that in skeletal myogenesis, gene expression is initiated by MyoD and includes the expression of specific Mef2 isoforms and activation of the p38 mitogen-activated protein kinase (MAPK) pathway.[35] In treated cells MyoD increased by about 26%, in comparison with controls (Fig. 1c), and was mainly distributed in the nuclear and perinuclear area (Fig. 1a and b). The increase in MyoD expression and the morphological changes in the cytoskeleton structure observed in treated cells strongly suggest that MLS laser radiation triggered a differentiation process in C2C12 cells.

### Effect of MLS laser treatment on cytoskeleton organization

The organization of the cytoskeleton network is a crucial factor in determining cell shape, regulating cell adhesion/migration, transducing signals and triggering intra and extracellular pathways. Therefore, the three major cytoskeleton components, *i.e.* actin microfilaments, microtubules and intermediate filaments were studied by immunofluorescence microscopy analysis. Control C2C12 cells showed the expected actin distribution (Fig. 2a): high expression in the perinuclear area, a clearly distinguishable "actin ring" close to the plasma membrane (arrow) and some stress fibers. After a cycle of three laser treatments the "actin ring" delimiting each individual cell disappeared. The cells tended to align and fuse to form tubes, filaments running parallel to the axis of the tubes appeared (arrows), the perinuclear area with high actin expression was thicker (Fig. 2b). The specific staining for tubulin revealed, in control cells, a radial distribution of the microtubules starting from the organization centre close to the nucleus (Fig. 2c). In treated samples a redistribution of the microtubules was observed: they were oriented parallel to the major axis of the cells and passed from one cell to another without interruption (arrows) (Fig. 2d). The intermediate filaments were studied by immunofluorescence staining of vimentin, which is their major constituent. The analysis of protein expression and distribution in control cells showed that the network of filaments was more dense in the perinuclear area, where it had the shape of a ball (Fig. 2e). In the cells treated with MLS laser, the intermediate filaments were parallel to the longitudinal axis of the cells (arrows), which appeared elongated and aligned to form tube-like structures (Fig. 2f).

In summary, C2C12 cells, subjected to MLS laser treatment, showed elongated shapes and were aligned and fused to form structures with two or more nuclei among which were no longer recognizable interposed membranes (tubes). These cytoarchitectural changes support the occurrence of a differentiation process[36] since the formation of a longitudinal microtubule array is an early event in myogenic differentiation.[37] It is also known that the reorganization of intermediate filaments and shifts from one to the other of the two major components, vimentin and desmin, occur during myogenesis.[38–40] Remodelling of actin
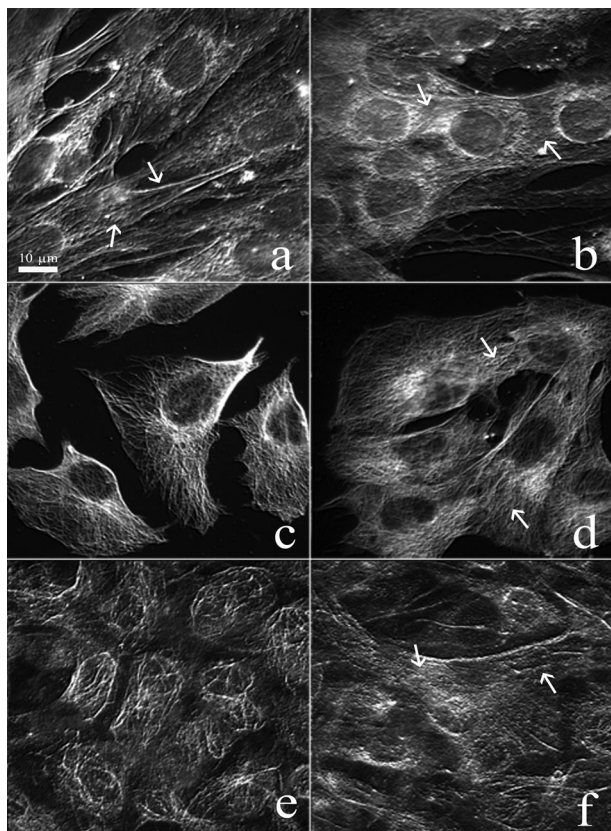
**Fig. 2** Cytoskeleton organization in C2C12 cells after MLS laser treatment. a, b: actin immunostaining. c, d: tubulin immunostaining. e, f: vimentin immunostaining. In control C2C12 cells (a) actin resulted highly expressed in the perinuclear area and formed a distinguishable ''actin ring'' close to the plasma membrane (arrows). Some stress fibers were present. After a cycle of three laser treatments (b) the ''actin ring'' delimiting each individual cell disappeared. The cells tended to align and fuse to form tubes, filaments running parallel to the axis of the tubes appeared (arrows), the perinuclear area with high actin expression was thicker. In control cells (c), microtubules showed a radial distribution starting from the organization centre close to the nucleus. In treated samples (d) the microtubules oriented parallel to the major axis of the cells and passed from one cell to another without interruption (arrows). In control cells (e), the network of intermediate filaments was more dense in the perinuclear area, where it had the shape of a ball. In laser treated cells (f), the intermediate filaments were parallel to the longitudinal axis of the cells (arrows), which appeared elongated and aligned to form tube-like structures.

microfilaments with the formation of stress fiber like structures has a very important role leading to myofibrillogenesis and is regulated by actin binding proteins[41] and phospholipase D.[42,43]

### Effect of MLS laser treatment on the proteome of C2C12 cells

In an attempt to identify the molecular changes induced by laser treatment of C2C12 cells, we have studied the protein expression pattern before and after laser treatment using 2-DE based proteomics. To ascertain the reproducibility of results 2-DE was performed three times for each protein sample. Fig. 3 shows a representative gel image. Image analysis using Progenesis Same Spot software allowed us to identify about 120 significantly (Anova $p$ value, $p \leq 0.05$) and consistently up- or down-regulated protein spots with fold changes greater than 1.5 in terms of

average normalised volumes in both triplicate gels of two independent experiments. Of these spots, 89 were up-regulated and 32 down-regulated in comparison to the control cells. Fig. 3 shows the significantly regulated spots, identified by MALDI-Tof mass spectrometry.

About eighty spots, corresponding to major protein variations, were cut from gels, destained, digested with trypsin and subjected to peptide mass fingerprinting followed by database searching. MALDI-TOF MS analysis allowed the unambiguous protein identification of 52 protein variations, corresponding to 42 proteins. Table 1 summarizes all the information obtained by protein identification. Protein numbering corresponds to that shown in Fig. 3. Swiss-Prot accession number and protein name are also included. The comparison between theoretical and measured molecular weight and pI values contributes to confirm the MASCOT search results in most cases. The MASCOT search results are reported in Table 1, showing experimentally measured peptide masses matching the theoretical ones from Swiss-Prot/UniProt entries, the percentage of the protein sequence covered by the matching peptides (sequence coverage), and the probabilistic score.

The identification of some protein spots, both selected as up-regulated proteins (spot No. 7, 13–15, 17, 40) and down-regulated ones (spot No. 4, 6, 37, 44), resulted in the same proteins: vimentin (spot No. 4, 13–15), actin γ (or β) (spot No. 17 and 44), tropomyosin α-3 chain (spot No. 6 and 40) and Rab GDP dissociation inhibitor β (spot No. 7 and 37). The position of these protein spots is clearly different. Fig. 4 shows details of the two-dimensional reference maps. Both tropomyosin α-3 chain and Rab GDP dissociation inhibitor β are associated with two spots with equal molecular weight but different isoelectric points. The observed shift in positions of these proteins could represent splice variants and/or post-translational modifications (*i.e.* phosphorylation) rather than an increase or decrease in the absolute amounts. Vimentin and actin γ (or β), identified by the analysis of protein spots up-regulated following laser treatment, have an apparent molecular weight higher than the theoretical one. This phenomenon was also observed for other proteins identified by the analysis of up-regulated protein spots. As we can note from Fig. 3 and Table 1, desmin (spot No. 16), pyruvate kinase isozymes M1/M2 (spot No. 22) and elongation factor 2 (spot No. 21) show a measured molecular weight higher than the theoretical one. We hypothesize that MLS laser treatment could induce the stabilization of pre-existing covalent polymeric species or their formation.

### Classification and functional analysis of modulated proteins

In order to gain insight into the biological significance of the proteins identified by proteomic analysis, the 42 differentially expressed proteins, identified by MALDI-Tof peptide mass finger printing of 52 isolated protein spots, were categorized according to the DAVID bioinformatics tool. Concerning biological processes, the identified proteins were distributed into categories; we report here the results obtained with the PANTHER (Protein Analysis Through Evolutionary relationships) classification system (Table 2). The main biological process in which the identified
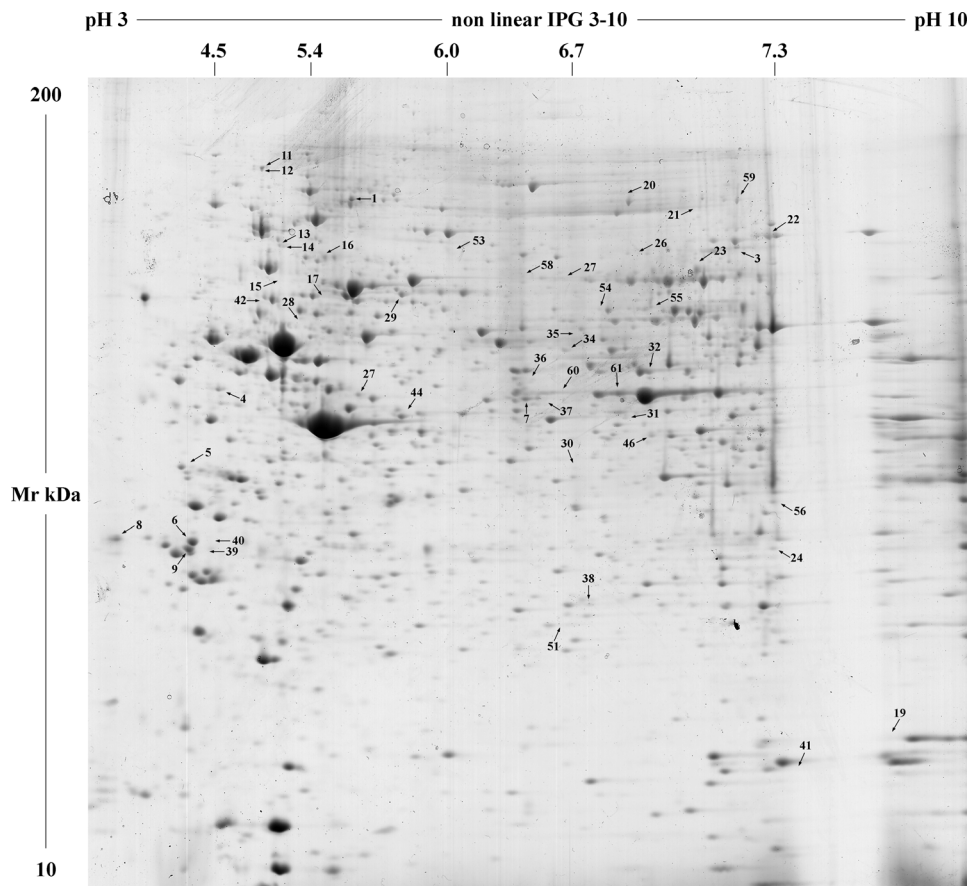
**Fig. 3** Representative reference 2-DE gel of C2C12 cells. Cell lysates of control C2C12 cells and MLS-treated C2C12 cells were resolved by 2-DE. IEF was carried out on nonlinear wide-range IPGs (pH 3–10; 18 cm IPG strips) and achieved using the Ettan™ IPGphor™ system. Sample load, 800 μg per strip, was successively performed by cup loading in the IPGphor Cup Loading Strip Holders. The second dimension was carried out on 9–16% polyacrylamide linear gradient gels (18 cm × 20 cm × 1.5 mm). Protein spots were visualized by colloidal coomassie blue staining. 2-DE gels were analysed using the Progenesis SameSpot software package. The arrows point to differential protein spots identified with the peptide-mass fingerprinting.

proteins were involved was "protein metabolism and modification" (38.1%), followed by "cell structure and motility" (28.6%), "carbohydrate metabolism" (11.9%), and "induction of apoptosis" (7.1%). The four tropomyosin isoforms identified and assigned to the "cell structure and motility" class can be categorized also in the "muscle contraction and development" class (not shown). Similarly heat shock proteins can be classified also as "stress response proteins". It is well known that the main function of the heat shock proteins is to provide thermotolerance and cytoprotection. Hsp-β1, up-regulated after MLS laser treatment, belongs to the small heat shock protein group. It is overexpressed during different stages of cell differentiation and development and it is thought to have an essential role in the differentiation processes of numerous tissues.[44]

The membership of most of the identified proteins to the class "protein metabolism and modification" clearly indicates a cellular response toward specific anabolic events, probably related to cytoskeleton network remodelling, leading to the morphological changes observed and described above. It is also remarkable that about 30% of the changes shown by proteomic analysis in laser treated samples concern proteins involved in cell structure and motility, such as actin γ/β, tropomyosin α and

β chains, vimentin, desmin, LIM domain and actin-binding protein, fascin, cofilin-1, many of which are actin-binding proteins and/or have been found to have a role in myogenesis. It has been demonstrated that the LIM domain and actin-binding protein increases when myoblasts are induced to differentiate and then progressively declines in myotubes.[45,46] Therefore, the increase in the LIM domain and actin-binding protein we observed fits with a scenario of differentiation at the early stages. Another interesting identified protein is α-enolase that results up-regulated after MLS laser treatment. Although it is clusterized into the class "carbohydrate metabolism", it is known that α-enolase is also involved in other cellular processes. It has been recently demonstrated that enolase isoforms interact with microtubules during muscle satellite cell differentiation contributing to the regulation of the cytoskeletal filaments dynamism that occurs during the transition from myoblasts to myotubes.[47,48] NLR family pyrin domain-containing protein 10 (NLRP 10), heterogeneous nuclear ribonucleoprotein K (HNRNP K) and galectin-3 following the PANTHER classification system were assigned to the "induction of apoptosis" class but they are also involved in other important processes.

**Table 1** Differentially expressed proteins identified by 2-DE coupled to MALDI-Tof MS analysis

| Spot no. | Accession no. | Protein names | MASCOT search results | | | Theoretical pI/Mr (kDa) | Measured pI/Mr (kDa) | Fold increase | ANOVA (p value) |
|---|---|---|---|---|---|---|---|---|---|
| | | | No. of matched peptides | Sequence coverage | Score | | | | |
| 1 | Q02053 | Ubiquitin-like modifier-activating enzyme 1 | 11 | 16 | 102 | 5.43/118.93 | 5.22/109.33 | −1.5 | 0.011 |
| 3 | Q8K1N2 | Pleckstrin homology-like domain family B member 2 | 12 | 9 | 80 | 7.58/142.25 | 6.97/103.90 | −1.6 | 0.025 |
| 4 | P20152 | Vimentin | 12 | 32 | 105 | 5.06/53.71 | 4.76/49.61 | −1.9 | 0.005 |
| 5 | P58774 | Tropomyosin β chain | 11 | 32 | 123[a] | 4.66/32.93 | 4.59/40.20 | −4.6 | 0.048 |
| 6 | P21107 | Tropomyosin α-3 chain | 13 | 39 | 104[a] | 4.68/32.90 | 4.64/32.85 | −4.6 | 0.048 |
| 7 | Q61598 | Rab GDP dissociation inhibitor β | 20 | 46 | 157 | 5.93/51.02 | 5.75/48.36 | −2.0 | 0.007 |
| 8 | O35658 | Complement component 1 Q subcomponent-binding protein | 4 | 28 | 60 | 4.82/31.34 | 4.30/33.18 | −2.9 | 0.008 |
| 9 | Q6IRU2 | Tropomyosin α-4 chain | 14 | 50 | 144 | 4.65/28.56 | 4.62/31.86 | −4.5 | 0.050 |
| 11 | P07901 | Heat shock protein, HSP 90-α | 17 | 26 | 82 | 4.93/85.13 | 4.91/n.d. | 2.9 | 0.050 |
| 12 | P11499 | Heat shock protein, HSP 90-β | 29 | 43 | 226 | 4.97/83.61 | 4.91/n.d. | | |
| 13 | P20152 | Vimentin | 26 | 57 | 226 | 5.06/53.71 | 5.03/105.51 | 5.7 | 0.048 |
| 14 | P20152 | Vimentin | 26 | 59 | 291 | 5.06/53.71 | 5.06/106.09 | 2.5 | 0.050 |
| 15 | P20152 | Vimentin | 7 | 21 | 71 | 5.06/53.71 | 5.03/81.78 | 2.5 | 0.031 |
| 16 | P31001 | Desmin | 21 | 44 | 195 | 5.21/53.52 | 5.22/96.91 | 1.5 | 0.033 |
| 16 | Q91VD9 | NADH-ubiquinone oxidoreductase 75 kDa subunit | 16 | 27 | 129 | 5.51/80.75 | 5.21/85.82 | 1.5 | 0.033 |
| 17 | Q6ZWM3 | Actin γ | 10 | 38 | 108 | 5.29/42.05 | 5.24/67.30 | 8.1 | 0.032 |
| | P63260 | Actin β | 10 | 38 | 108 | 5.31/42.11 | | | |
| 19 | P18760 | Cofilin-1 | 6 | 57 | 80 | 8.22/18.78 | n.d./19.93 | 1.9 | 0.050 |
| 20 | Q3TL91 | Rho GTPase-activating protein 31 | 13 | 12 | 72 | 5.58/156.55 | 6.28/166.41 | 1.7 | 0.031 |
| 21 | P58252 | Elongation factor 2 | 20 | 42 | 203 | 6.41/96.22 | 6.74/151.03 | 1.9 | 0.031 |
| 22 | Q91YI8 | Pyruvate kinase isozymes M1/M2 | 12 | 32 | 138 | 7.18/58.38 | 7.17/120.36 | 3.4 | 0.022 |
| 23 | Q9ERG0 | LIM domain and actin-binding protein 1 | 23 | 27 | 133 | 6.18/84.66 | 6.70/93.27 | 1.8 | 0.034 |
| 24 | P16110 | Galectin-3 | 8 | 34 | 110 | 8.46/27.61 | n.d./33.13 | 3.2 | 0.042 |
| 25 | P56399 | Ubiquitin specific peptidase 5 | 7 | 7 | 81 | 4.89/96.68 | 6.48/96.08 | 3.2 | 0.004 |
| 26 | Q9ERG0 | LIM domain and actin-binding protein 1 | 18 | 26 | 119 | 6.18/84.66 | 6.36/96.49 | 4.6 | 0.049 |
| 27 | P60843 | Eukaryotic initiation factor 4A-I | 14 | 48 | 191 | 5.32/46.35 | 5.38/48.61 | 1.5 | 0.015 |
| 28 | P61979 | Heterogeneous nuclear ribonucleoprotein K | 10 | 23 | 109 | 5.39/51.23 | 5.14/59.29 | 1.5 | 0.028 |
| 29 | Q61696 | Heat shock protein, HSP 70 | 12 | 25 | 123 | 5.53/70.32 | 5.48/69.42 | 2.6 | 0.001 |
| 30 | P62141 | PP1-β catalytic subunit | 10 | 36 | 94 | 5.84/37.96 | 5.80/42.44 | 1.9 | 0.002 |
| 31 | P50580 | Proliferation-associated protein 2G4 | 14 | 51 | 169 | 6.41/44.01 | 6.57/48.61 | 2.9 | 0.049 |
| 32 | Q61553 | Fascin | 12 | 34 | 148 | 6.44/55.22 | 6.64/52.38 | 1.6 | 0.033 |
| 34 | P80314 | T-complex protein 1 subunit β | 15 | 35 | 171 | 5.97/57.78 | 6.29/55.47 | 1.5 | 0.050 |
| 35 | P26638 | Seryl-tRNA synthetase | 21 | 45 | 239 | 5.95/58.86 | 6.37/57.87 | 1.8 | 0.005 |
| 36 | Q62465 | Synaptic vesicle membrane protein VAT-1 homolog | 6 | 21 | 68 | 5.95/43.30 | 5.79/50.91 | 2.4 | 0.005 |
| 37 | Q61598 | Rab GDP dissociation inhibitor β | 9 | 27 | 83 | 5.93/51.02 | 5.84/48.49 | 2.1 | 0.010 |
| 38 | P14602 | Heat shock protein, HSP β-1 | 10 | 50 | 122 | 6.12/23.06 | 6.08/27.93 | 4.1 | 0.004 |
| 39 | P58771 | Tropomyosin α-1 chain | 15 | 45 | 165 | 4.69/32.72 | 4.75/32.39 | 3.5 | 0.049 |
| 40 | P21107 | Tropomyosin α-3 chain | 9 | 21 | 157[a] | 4.68/32.90 | 4.68/31.75 | 5.8 | 0.029 |
| 41 | P17742 | Peptidyl-prolyl cis–trans isomerase A | 6 | 42 | 107 | 7.74/18.13 | n.d./17.35 | 8.6 | 0.022 |
| 42 | Q9JIG7 | Coiled-coil domain-containing protein 22 | 9 | 18 | 71 | 5.71/71.26 | 5.00/67.81 | −1.8 | 0.016 |
| | Q6ZWM3 | Actin γ | 8 | 26 | 73 | 5.29/42.05 | 5.58/46.10 | −2.3 | 0.008 |
| 44 | P63260 | Actin β | 8 | 26 | 73 | 5.31/42.11 | | | |
| 46 | Q61990 | Poly(rC)-binding protein 2 | 7 | 28 | 81 | 6.33/38.60 | 6.66/43.85 | −1.5 | 0.023 |
| 51 | P43025 | Tetranectin | 5 | 24 | 74 | 5.50/22.64 | 6.27/26.31 | 3.1 | 0.007 |
| 53 | Q8CCN1 | NLR family, pyrin domain-containing protein 10 | 21 | 29 | 159 | 6.18/72.29 | 5.79/87.84 | 3.1 | 0.008 |
| 54 | O08553 | Dihydropyrimidinase-related protein 2 | 14 | 37 | 172 | 5.95/62.64 | 6.42/65.412 | 1.8 | 0.050 |
| 55 | Q9CWJ9 | Bifunctional purine biosynthesis protein | 12 | 35 | 174 | 6.30/64.69 | 6.64/66.09 | 1.6 | 0.034 |
| 56 | P06151 | L-Lactate dehydrogenase A chain | 13 | 34 | 131 | 7.62/36.82 | 7.36/36.55 | 2.4 | 0.033 |
| 58 | Q8R4K2 | Interleukin-1 receptor-associated kinase 4 | 9 | 25 | 100 | 5.23/51.41 | 5.78/83.51 | 5.2 | 0.012 |
| 59 | P58252 | Elongation factor 2 | 8 | 12 | 70 | 6.41/96.22 | 6.15/78.39 | 2.9 | 0.050 |
| 60 | P17182 | α-Enolase | 13 | 45 | 153 | 6.37/47.45 | 6.28/49.47 | 4.4 | 0.031 |
| 61 | P17182 | α-Enolase | 17 | 55 | 212 | 6.37/47.45 | 6.41/49.22 | 1.5 | 0.023 |

[a] The number of accepted missed cleavage sites was set to two.

NLRP 10 is one of 14 pyrin domain containing members of the NOD-like receptor family of cytoplasmic receptors. It is an intracellular protein involved not only in apoptosis but also in the immune system function. In fact it is believed that NLRP 10 helps to regulate the inflammatory response. NLRP 10 reduces inflammatory and innate immune responses by inhibiting the activity of two proteins associated with the inflammasome: caspase-1 and PYCARD.[49,50] Although the increase in NLRP 10 found after laser treatment does not seem to be connected to differentiation, it could represent one of the mechanisms underlying the anti-inflammatory effect attributed to the laser therapy.
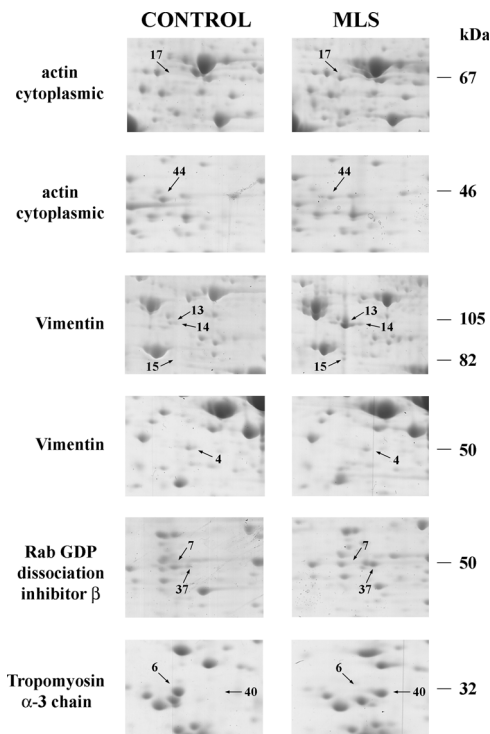
**Fig. 4** Protein shift position of actin γ (or β), vimentin, tropomyosin α-3 chain, and Rab GDP dissociation inhibitor β upon MLS-treatment of C2C12 cells. The panels show the regions, selected by representative 2-DE gels, with actin γ (or β), vimentin, tropomyosin α-3 chain, and Rab GDP dissociation inhibitor β localization. The indicated proteins shift their position in response to MLS-treatment due, likely, to post-translational modification.

HNRNP K belongs to the subfamily of heterogeneous nuclear ribonucleoproteins (hnRNPs). These proteins are associated with pre-mRNAs in cell nucleus and are known to influence pre-mRNA processing and other aspects of mRNA metabolism and transport. Experiments on animal models showed that HNRNP K is required for axonogenesis during development and several of its RNA targets are under strong post-transcriptional control during the regeneration process.[51] The increase in HNRNP K observed in laser treated cells could be an intriguing starting point for future research, since it has been shown that IR laser therapy promotes the regeneration of nerve fibers.[52] HNRNP K is also thought to have a role in cell cycle progression,[53] therefore the increase in expression could also be connected with the beginning of a differentiation process.

Galectin-3 plays a key role in several intracellular and extracellular processes. Documented intracellular functions are the regulation of cell growth, apoptosis and cell cycle.[54] Extracellular function consists in mediating/modulating cell to extracellular matrix adhesive interactions. Recent studies indicate galectin-3 as a mediator of signal transduction events on the cell surface as well as a mediator of a variety of extracellular processes such as angiogenesis, neuronal functions, endocytosis and possibly exocytosis.[55]

Finally, we would like to highlight the identification of PP1 as one of the up-regulated proteins in MLS laser treated cells.

Interestingly the PP1 catalytic subunit protein is included in each of the three main classes. PP1 is a major eukaryotic protein serine/threonine phosphatase that regulates an enormous variety of cellular functions through specific associations with regulatory subunits. PP1, primarily known for its role in the carbohydrate metabolism, actually regulates functions such as actin and actomyosin reorganization, cell shape and cell adhesion, muscle contraction/relaxation.[56]

To assess the identity of PP1 we performed an immunoblot analysis using a specific anti-PP1 antibody. Actin and enolase were selected to undergo a confirmatory test as well. Fig. 5 shows immunoblot results in comparison with the colloidal coomassie staining. Western blot analysis also confirms the up-regulation of enolase and the up-regulation of PP1 in laser treated cells, according to 2-DE gel image analysis.

Another interesting aspect highlighted by the DAVID classification system as a function of the keywords is that 81% of the identified proteins are classified as "phosphoproteins" (Table 3). Some of these proteins actually are PP1 substrates or interact with it (i.e. cofilin,[57] heterogeneous nuclear ribonucleoprotein K,[58] enolase,[59] heat shock proteins,[60,61] peptidyl-prolyl isomerase,[62] vimentin[63,64]).

The overexpression of cofilin is notable. Cofilin is a protein associated with the cytoskeleton that binds actin and reversibly controls polymerization and depolymerization in a pH-sensitive manner; the ability of cofilin to control actin polymerization is known to be regulated by reversible phosphorylation.[65] Cofilin is phosphorylated by LIM kinase 1, which abolishes its ability to de-polymerize actin, and dephosphorylated by PP1 and PP2A.[66] PP1 and PP2A play an important role in myoblast differentiation. It has been shown that inhibition of PP1 and PP2A by okadaic acid blocks myogenesis by altering the MyoD binding activity[67] and depletion of PP1 abolishes the ability of myoblasts to differentiate into myotubes.[68] Proteomic analysis of samples exposed to MLS laser treatments for 3 consecutive days showed an increase in PP1 but no significant changes in PP2A. This finding completely agrees with the results of other authors, who examined PP1 and PP2A activities during various stages of myogenesis in rat skeletal muscle cells. PP1 activity increased progressively in cultures from 2 to 5 days, PP2A activities remained constant in days 2–4 cultures and increased sharply on day 5.[69] An indirect proof of the key role played by PP1 in muscle homeostasis is the decrease of PP1 levels, associated with a decrease in metabolic enzymes, observed in hypotrophic and sarcopenic muscles.[70]

Finally it is also relevant that 28.7% of the identified proteins are "ATP-binding proteins", 19% are "coiled coil proteins" and 16.7% "actin-binding proteins". The increased availability of ATP induced by exposure to the red-IR laser radiation[71] could be correlated with the net increase of proteins capable of binding ATP. Changes in the expression of actin-binding proteins, as well as those in typical intermediate filament proteins (here classified in part as "coiled coil" proteins), are events related to the general cytoskeletal rearrangement also observed by fluorescence microscopy (Fig. 2).

**Table 2** Predominant biological processes associated with LMS-treatment when compared to control C2C12 cells as provided by DAVID (Database for Annotation, Visualization and Integrated Discovery; http://david.abcc.ncifcrf.gov), using the PANTHER classification system. ↑: up-regulated proteins; ↓: down-regulated proteins; ↓/↑: proteins identified from multiple protein spots (both up-regulated and down-regulated). The italicized proteins are present in more than one functional class

| Protein metabolism, modification 38.1% | | Cell structure and motility 28.6% | | Carbohydrate metabolism 11.9% | | Induction of apoptosis 7.1% | | Not classified 19% | |
|---|---|---|---|---|---|---|---|---|---|
| T-complex protein 1 subunit β | ↑ | LIM domain and actin-binding protein 1 | ↑ | Pyruvate kinase | ↑ | NLR family, pyrin domain-containing protein 10 | ↑ | Bifunctional purine biosynthesis protein | ↑ |
| *Heterogeneous nuclear ribonucleoprotein K* | ↑ | Cofilin-1 | ↑ | L-Lactate dehydrogenase | ↑ | *Heterogeneous nuclear ribonucleoprotein K* | ↑ | Dihydropyrimidinase-related protein 2 | ↑ |
| Interleukin-1 receptor-associated kinase 4 | ↑ | Desmin | ↑ | *PP1-β* | ↑ | Galectin-3 | ↑ | NADH-ubiquinone oxidoreductase | ↑ |
| Eukaryotic initiation factor 4 A-I | ↑ | Fascin | ↑ | Synaptic vesicle membrane protein VAT-1 | ↑ | | | Rab GDP dissociation inhibitor β | ↑ |
| Peptidyl-prolyl *cis–trans* isomerase A | ↑ | Tropomyosin α-1 | ↑ | α-Enolase | ↑ | | | Rho GTPase-activating protein 31 | ↑ |
| Proliferation-associated protein 2G4 | ↑ | *PP1-β* | ↑ | | | | | Coiled-coil domain-containing protein 22 | ↓ |
| Seryl-tRNA synthetase | ↑ | Tropomyosin β | ↓ | | | | | Pleckstrin homology-like domain family B member 2 | ↓ |
| Ubiquitin specific peptidase 5 | ↑ | Tropomyosin α-4 | ↓ | | | | | Complement component 1 Q subcomponent-binding protein | ↓ |
| HSP 90-α | ↑ | Vimentin | ↓/↑ | | | | | | |
| HSP 90-β | ↑ | Actin γ | ↓/↑ | | | | | | |
| HSP β-1 | ↑ | Actin β | ↓/↑ | | | | | | |
| HSP 70 | ↑ | Tropomyosin α-3 | ↓/↑ | | | | | | |
| *PP1-β* | ↑ | | | | | | | | |
| Elongation factor 2 | ↑ | | | | | | | | |
| Poly(rC)-binding protein 2 | ↓ | | | | | | | | |
| Ubiquitin-like modifier-activating enzyme 1 | ↓ | | | | | | | | |
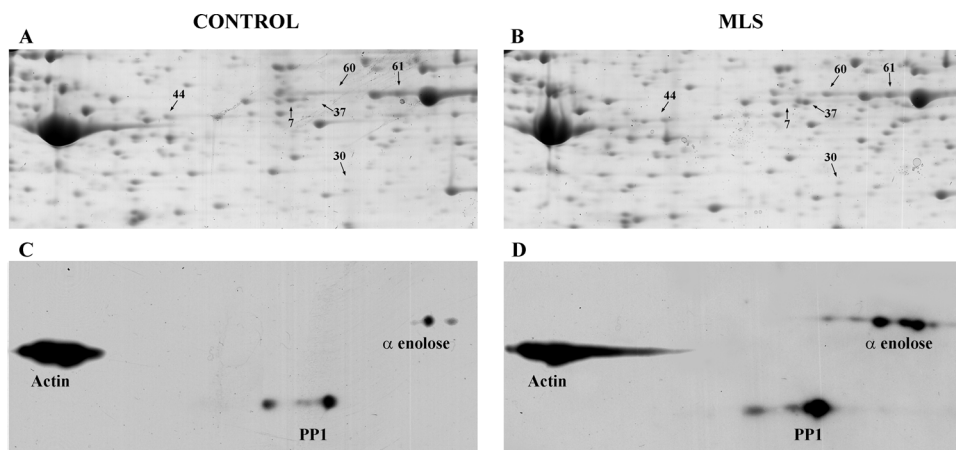


**Fig. 5** Validation of the PP1 identity by immunoblot analysis. 100 μg of protein extracts from control and MLS treated C2C12 cells were separated by 2-DE and transferred on a PVDF membrane. The blots were incubated with anti-PP1 antibody. Anti-actin and anti-enolase antibodies were used as loading and position control. Blots were visualized by autoradiography (c, d). The panels represent the 2-DE selected regions in which localize PP1, actin and enolase. The upper panels (a, b) show the colloidal coomassie blue stained gels.

## MLS laser treatment induces a significative PPPs activity increase

The identification of PP1 as one of the up-regulated proteins in response to MLS laser treatment and the observation that 81% of the identified proteins are proteins whose function depends on the phosphorylation status led us to investigate whether there were changes in the total cellular protein serine/threonine phosphatases activity. PPPs activity assays, performed on cell lysates obtained after MLS laser treatment of C2C12 cells, show a 1.8 fold increase with respect to untreated cells (Fig. 6) confirming the importance of specific phosphorylation/dephosphorylation events in maintaining the integrity of intermediate filaments[63–65,72] and other fundamental biological functions.[73–76] Fig. 6 shows the results obtained for other enzymes: lactate dehydrogenase, enolase and pyruvate kinase. All these proteins are overexpressed after MLS laser treatment and show an increase in their enzymatic activity.

**Table 3** Predominant keywords associated with identified proteins as provided by DAVID (Database for Annotation, Visualization and Integrated Discovery; http://david.abcc.ncifcrf.gov). ↑: up-regulated proteins; ↓: down-regulated proteins; ↓/↑: proteins identified from multiple protein spots (both up-regulated and down-regulated). The italicized proteins are present in more than one category

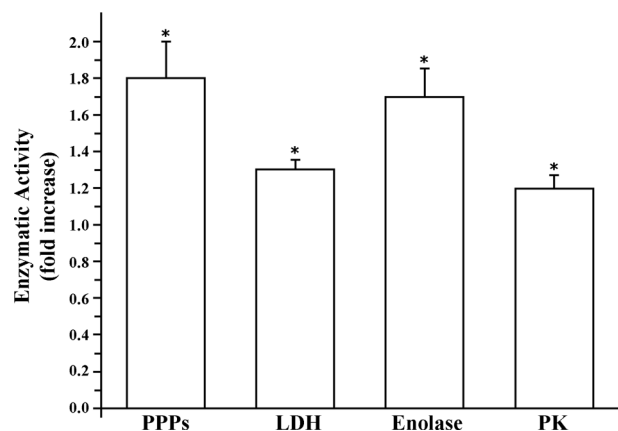| Phosphoprotein 81% | ATP-binding protein 28.6% | Coiled coil 19% | Actin-binding protein 16.7% | Stress-response 9.5% | Not classified 9.5% |
|---|---|---|---|---|---|
| Eukaryotic translation elongation factor 2 ↑ | Ubiquitin specific peptidase 5 ↑ | *Coiled-coil domain containing 22* → | *LIM domain and actin binding 1* ↑ | *HSP β-1* ↑ | Rab GDP dissociation inhibitor β ↑ |
| Rho GTPase-activating protein 31 ↑ | Heterogeneous nuclear ribonucleoprotein K ↑ | Pleckstrin homology-like domain, family B, member 2 → | *Cofilin 1* ↑ | HSP 70 ↑ | Synaptic vesicle membrane protein VAT-1 homolog ↑ |
| LIM domain and actin binding 1 ↑ | *Eukaryotic translation initiation factor 4A1* ↑ | *Tropomyosin β* → | *Fascin homolog 1* ↑ | *HSP 90-α* ↑ | NADH-ubiquinone oxidoreductase ↑ |
| Complement component 1 Q subcomponent-binding protein → | *Seryl-aminoacyl-tRNA synthetase* → | *Tropomyosin α-4* → | *Tropomyosin α-1* ↑ | *HSP 90-β* ↑ | Tetranectin ↑ |
| Interleukin-1 receptor-associated kinase 4 ↑ | *Interleukin-1 receptor-associated kinase 4* → | *Tropomyosin α-1* ↑ | *Tropomyosin β* → | | |
| Ubiquitin-like modifier activating enzyme 1 → | *HSP 90-α* → | *Tropomyosin α-3* ↓/↑ | *Tropomyosin α-4* → | | |
| Seryl-aminoacyl-tRNA synthetase ↑ | *HSP 90-β* ↑ | *Vimentin* ↓/↑ | *Tropomyosin α-3* ↓/↑ | | |
| Cofilin 1 ↑ | *HSP β-1* ↑ | Desmin ↑ | | | |
| Fascin homolog 1 ↑ | *Pyruvate kinase* ↑ | | | | |
| Galectin-3 ↑ | *Actin γ/actin β* ↑ | | | | |
| L-Lactate dehydrogenase ↑ | *Ubiquitin-like modifier activating enzyme 1* → | | | | |
| α-Enolase ↑ | | | | | |
| Proliferation-associated 2G4 ↑ | | | | | |
| *HSP β-1* ↑ | | | | | |
| *HSP 90-α* ↑ | | | | | |
| *HSP 90-β* → | | | | | |
| *Vimentin* ↓/↑ | | | | | |

**Fig. 6** Enzymatic assays of some overexpressed proteins and cellular protein phosphatases. The enzymatic activity of protein serine/threonine phosphatases (PPPs), lactate dehydrogenase (LDH), enolase, and pyruvate kinase (PK) was determined in cell lysates by specific tests. The figure shows the activity fold increase observed in MLS-treated C2C12 cells with respect to control cells. Results shown represent means of two experiments in duplicate (SEM (*$p \leq 0.05$)).

## Experimental

### Cell culture

Murine myoblasts (C2C12 skeletal muscle cell line) were routinely cultured in growing medium consisting of Dulbecco's Modified Eagle's Medium supplemented with 100 μg ml$^{-1}$ streptomycin, 100 U ml$^{-1}$ penicillin, 2 mM glutamine and 10% fetal bovine serum (FBS). Cells were incubated at 37 °C and 5% CO$_2$. All the reagents for cell culture were purchased from Sigma Chemical Co. (St Louis, MO, USA).

### MLS laser treatment

The treatments have been performed with a Multiwave Locked System (MLS) laser (ASA Srl, Vicenza, Italy), a device already used for some years in clinics (FDA approved and CE certified instrument) and specifically applied in physical medicine and pain therapy. It is a high power (average power up to 1.1 W, class IV) IR laser with two synchronized sources (laser diodes). The two modules have different wavelengths, peak power and emission mode. The first one is a pulsed laser diode, emitting at 905 nm, with a peak optical power = 25 W; each pulse is composed of a pulse train (single pulse width = 100 ns, maximum frequency 90 kHz), thus varying the average power delivered to the tissue. The frequency of the pulse trains may be varied in the range 1–2000 Hz. The second laser diode (808 nm) operates in continuous mode (power 1.1 W) or in pulsed mode (pulses repetition rate 1–2000 Hz), mean optical power output = 550 mW, duty ratio 50% independent of the pulse repetition rate. The two propagation axes are coincident.

For the treatment, cells were seeded in the central 8 wells of a 24-multiwall plate. The plate was placed inside a plexiglass support, specifically designed and built. On the top of the support there was a central groove in which the laser handpiece slided. The plate was perfectly aligned with the handpiece, at a distance of 3 cm from it, so that the spot formed by the two superimposed laser beams had a diameter equal to that of a single well (13 mm). The support allowed us to perform a homogeneous scan of 8 samples at the same time, by moving the spot at a constant horizontal velocity above the 8 treated wells (5.6 cm s$^{-1}$: each scan of 8 wells lasted 20 s), in order to have the same radiant energy impinging into each well ($\sim$68 J for the whole treatment). Treatment parameters were 1500 Hz frequency and 8 min total scan time. The scan mode is also extensively used in clinics because it allows us to treat easily larger areas and, together with the other treatment parameters chosen, contributes to achieve the desired effects avoiding any side effects.

The treatment was repeated once a day, for 3 consecutive days under sterile conditions. The treated samples were compared with controls maintained under the same conditions, except for the laser exposure.

### Viability and proliferation

Cell viability was assessed by the Trypan Blue assay after a single exposure and 3 exposures (once a day for 3 consecutive days) to MLS treatment. The treated samples were compared to untreated controls. After the MLS treatment, the samples were washed and cell detachment was obtained by treating with trypsin–EDTA for 3–4 minutes. Then the cells were centrifuged and resuspended in a solution of phosphate buffered saline (PBS) and Trypan Blue (dilution factor: 2). The dye is able to penetrate selectively into dead cells. After 5 min of incubation, cell counts were performed by using a Neubauer haemocytometer.

### Immunofluorescence analysis

At the end of the experiments, cells were fixed for 5 min in cold acetone, then washed in phosphate buffered saline (PBS). After blocking unspecific binding with PBS containing 3% bovine serum albumin, cells were incubated overnight at 4 °C with the specific anti-MyoD (Santa Cruz Biotechnology, SC-32758), anti-α-actin (Millipore, MAB1501X), anti-tubulin (Upstate Biotechnology, 05829) and anti-vimentin (Chemicon, MAB1681) antibodies. The cells were then incubated with the fluorescein isothiocyanate (FITC) conjugated specific secondary antibodies (specifically: anti-mouse IgG (Chemicon Int, AP 124-T) for anti-tubulin antibody and anti-mouse IgM (Chemicon Int, AP 132-T) for anti-vimentin antibody). Cells incubated with anti-α actin antibody did not need incubation with the secondary antibody since a mouse anti-actin Alexa Fluor® 488 conjugated was used. Negative controls were obtained by omitting the primary antibodies. Samples were evaluated using an epifluorescence microscope (Nikon, Florence, Italy) at 100× magnification and imaged by a HiRes IV digital CCD camera (DTA, Pisa, Italy).

Image analysis was performed by extracting, for each cell image, the region of interest (ROI) by appropriate software (Image Pro Plus). Then, the mean pixel value (16 bit, gray level) related to the mean fluorescence intensity and therefore to the specific epitope detection was calculated.

### Data analysis

Three different experiments were carried out in triplicate. For viability and proliferation assays at least 10 counts per sample were carried out and the mean value was calculated.

For immunofluorescence analysis, at least 30 cells per slide were scored in 10 random fields per slide, and the data were expressed as mean $\pm$ SD. Statistical significance was determined using a Student's $t$-test. A $p$ value lower than 0.05 was considered statistically significant.

## Proteomic sample preparation and 2-DE

For 2-DE, MLS treated and control cells were harvested by centrifugation at room temperature. The pellet was washed twice in water and resuspended in 8 M urea, 4% CHAPS, and 10 mM DTT. After sonicating briefly, protein extracts were clarified by centrifugation at $14\,000 \times g$ for 10 min. The protein concentration of each purified sample was determined using the 2D Quant kit (GE Healthcare, USA). For each experimental condition 2-DE replicate gels ($n = 3$) were made using independent experiments, in order to assess biological and analytical variations. IEF (first dimension) was carried out on nonlinear wide-range IPGs (pH 3–10; 18 cm long IPG strips; GE Healthcare, Uppsala, Sweden) and achieved using the Ettan™ IPGphor™ system (GE Healthcare). IPG-strips were rehydrated with 350 µl of lysis buffer and 2% v/v carrier ampholyte, for 12 h at room temperature. Sample load, 800 µg per strip, was successively performed by cup loading in the IPGphor Cup Loading Strip Holders (GE Healthcare), with the sample cup system at the anodic side of IPG strips. IEF was then achieved according to the following voltage steps, at 20 °C: 30 V for 30 min, 200 V for 2 h, 500 V for 2 h, from 500 to 3500 V for 30 min, 3500 V for 5 h, from 3500 to 5000 V for 30 min, 5000 V for 4 h, from 5000 to 8000 V for 30 min, 8000 V until a total of 95 000 V h⁻¹ was reached. After focusing, prior to the second-dimension separation, IPG strips were equilibrated in equilibration buffer (6 M urea, 75 mM Tris–HCl pH 8.8, 29.3% glycerol, 2% SDS) containing 1% (w/v) DTT for 15 min and then in the same equilibration buffer containing 2.5% iodoacetamide for a further 15 min.

The second dimension separation was carried out on 9–16% polyacrylamide linear gradient gels (18 cm × 20 cm × 1.5 mm) at 40 mA per gel constant current and 10 °C until the dye front reached the bottom of the gel.[77] Protein spots were visualized by colloidal coomassie blue staining.[78] The stained gels were scanned with the Epson Expression 1680 Pro image scanner.

## Image analysis

Scanned images (16-bit grayscale) were processed and statistically evaluated with Progenesis SameSpots software (Nonlinear Dynamics, Newcastle upon Tyne, UK). Both manual and automatic alignment was used to align the images. A control group and a "laser treated" group containing three technical replicates were created and only spots present in all the replicates were taken into consideration for subsequent analysis. The two groups were compared with each other and fold values as well as $p$-values of all spots were computed by the above-mentioned software using one way ANOVA analysis. All spots were prefiltered and manually checked before applying the statistical criteria (Anova $p \leq 0.05$ and fold $\geq 1.5$). Normalized spot volumes, instead of spot intensity, were used in statistical processing. Protein identification involved only spots that fulfilled the statistical criteria. Experimental pI and $M_w$ values

were estimated using MW protein markers and some identified proteins selected as markers.

## In-gel digestion and MALDI-TOF analysis

Protein spots were manually excised from gels and each sample was transferred to a 1.5 ml Eppendorf tube, washed twice in 50 mM ammonium bicarbonate ($NH_4HCO_3$)/$CH_3CN$ 1/1 for 15 min and then de-hydrated in $CH_3CN$. Dried samples were re-swelled in $NH_4HCO_3$ containing 10 mM DTT (freshly prepared) and incubated for 30 min at 56 °C; the excess liquid was then removed and replaced with the same volume of freshly prepared 55 mM IAA in 25 mM $NH_4HCO_3$. After 30 min of incubation at room temperature in the dark, the gel particles were washed twice with $NH_4HCO_3$/$CH_3CN$ 1/1 for 15 min, de-hydrated in $CH_3CN$ and dried in a vacuum centrifuge. Each sample was incubated for 1 h at 37 °C in 20 µl of 20 µg ml⁻¹ trypsin solution (Trypsin Proteomics Sequencing Grade T6567, SIGMA) in 40 mM $NH_4HCO_3$ with 10% $CH_3CN$. An additional 30 µl of 40 mM $NH_4HCO_3$ with 10% $CH_3CN$ were added to each sample and incubated overnight at 37 °C. The reaction was stopped by adding a final concentration of 0.1% trifluoroacetic acid. The supernatant was collected and the gel was further extracted with 0.1% trifluoroacetic acid in 50% $CH_3CN$.[79,80] The extracts were combined and then analysed on a MALDI-TOF/TOF mass spectrometer Ultraflex III (Bruker Daltonics, Bremen, Germany) by using Flex Control 3.0 as data acquisition software. A 0.75 µl volume of the sample was mixed with 0.75 µl of the matrix (saturated solution of α-cyano-4-hydroxycinnamic acid in 50% (v/v) $CH_3CN$ and 0.5% (v/v) TFA) on the anchorchip target plate and allowed to dry. Spectra were acquired in the reflectron mode over the $m/z$ range 860–4000 for a total of 500 shots. The instrumental parameters were chosen by setting the ion source 1 at 25 kV, ion source 2 at 21.5 kV, the pulsed ion extraction at 20 ns and the detector gain at 7.7×. The instrument was externally calibrated prior to analysis using the Bruker Peptide Calibration standard kit. All the resulting mass lists were cleaned up from eventually present contaminant masses, such as those from matrix, autodigestion of trypsin and keratins. Mass fingerprinting searching was carried out in Swiss-Prot/TrEMBL databases using MASCOT (Matrix Science Ltd., London, UK, http://www.matrixscience.com) software. The taxonomy was restricted to *Mus musculus*, a mass tolerance of 50 ppm was allowed, and the number of accepted missed cleavage sites was set to one. Alkylation of cysteine by carbamidomethylation was assumed as fixed modification. The experimental mass values were monoisotopic. No restrictions on protein molecular weight and pI were applied. The criteria used to accept identifications included the extent of sequence coverage, number of matched peptides and probabilistic score sorted by the software.

## Western blot

Western blot analysis was performed to validate the identity and the differential expression of PP1, enolase and actin. 100 µg of protein extracts from control and MLS treated C2C12 cells were separated by 2-DE as previously described and transferred

onto a PVDF membrane (Millipore). The blots were incubated with anti-actin (Santa Cruz Biotechnology, SC-1615), anti-enolase (Santa Cruz Biotechnology, SC-7455) and anti-PP1 antibodies (Santa Cruz Biotechnology, SC-7482) in blocking buffer (PBS, 2% nonfat dry milk, 0.1% v/v Tween-20). After incubation with secondary antibodies, the blotting was developed by using the ECL plus immunodetection system ECL (GE Healthcare) and visualized by autoradiography.

### Cluster analysis

The differentially expressed proteins were subjected to functional pathway analysis using DAVID database (http://david.abcc.ncifcrf.gov/home.jsp)[81] for better understanding of the biological context of the identified proteins and their participation in various physiological processes. UniProt accession numbers of the 42 differentially expressed proteins identified in our study were uploaded and mapped against the *Mus musculus* reference dataset to extract and summarize functional annotation associated with individual or group of genes/proteins and to identify gene ontology terms, molecular function, biological process and important pathways for each dataset.

### Determination of protein serine phosphatases, pyruvate kinase, enolase and lactate dehydrogenase activities

Protein Serine Phosphatases (PPPs) activity was determined in C2C12 cell lysates from three independent experiments. MLS-treated and not treated C2C12 cells were quickly rinsed in ice-cold phosphate-buffered saline (PBS, 10 mM sodium phosphate and 0.15 M NaCl, pH 7.2), and freezed. After thawing the material at room temperature, the lysis was performed at 4 °C in 50 mM Tris, pH 7.4, containing 5 mM dithiothreitol and Sigma protease inhibitors mix (1/100, v/v). After 30 min of incubation on ice, lysates were sonicated (three short bursts) and centrifuged at 12 000$g$ in a microcentrifuge at 4 °C for 30 min. Supernatants were quantified with respect to proteins content by the Bradford method. PPPs activity was determined using $p$-nitrophenyl phosphate as the substrate. All enzymatic activity tests were performed in duplicate. The substrate (4 mM) was dissolved in 25 mM Tris–HCl buffer, pH 7.2, containing 5 mM dithiothreitol, 20 mM sodium–potassium DL-tartrate and 0.1 mM sodium orthovanadate. Tartrate and orthovanadate were added in order to inhibit protein tyrosine phosphatases, lysosomal acid phosphatases and non-specific phosphatases.[82,83] The reaction was stopped with 0.1 M KOH and the released $p$-nitrophenolate ion was measured by reading the absorbance at 400 nm ($\varepsilon = 18\,000$ M$^{-1}$ cm$^{-1}$). The activity measured under these conditions was completely inhibited by 0.01 mM cantharidic acid, a specific and strong inhibitor of all PPPs.[84] Statistical significance was determined using a Student's $t$-test. A $p$ value lower than 0.05 was considered statistically significant.

Pyruvate kinase (PK) activity was determined at 30 °C according to Bergmeyer,[85] with slight modifications, continuously following the NADH oxidation at 340 nm, using an UV-2100 spectrophotometer (Shimadzu, Columbia, MD). The assay mixture contained in 1 ml final volume consisted of 50 mM triethanolamine (pH 7.6), 8 mM MgSO$_4$, 5 mM EDTA, 75 mM KCl, 1.5 mM ADP, 0.15 mM NADH, 60 units of lactate dehydrogenase. The reaction was started by adding substrate (0.8 mM phosphoenolpyruvate). Enolase activity was determined at 30 °C according to Bergmeyer,[86] with slight modifications, continuously following the NADH oxidation at 340 nm, using an UV-2100 spectrophotometer (Shimadzu, Columbia, MD). The assay mixture contained in 1 ml final volume consisted of 80 mM triethanolamine (pH 7.6), 3.3 mM MgSO$_4$, 1.1 mM ADP, 0.2 mM NADH, 20 units of lactate dehydrogenase, 3 units of pyruvate kinase. The reaction was started by adding substrate (0.9 mM phosphoglycerate). Lactate dehydrogenase (LDH) activity was determined at 30 °C according to Bergmeyer,[87] with slight modifications, continuously following the decrease of NADH at 340 nm, using an UV-2100 spectrophotometer (Shimadzu, Columbia, MD). The assay mixture, contained in 1 ml final volume, consisted of 100 mM phosphate buffer pH 7.0 and 0.2 mM NADH. The reaction was started by adding substrate (0.77 mM pyruvate). The value of 6.22 mM$^{-1}$ cm$^{-1}$ is considered to be the NADH molar extinction coefficient. One unit of activity is defined as that quantity of enzyme which transforms one μmole of substrate in one minute at 30 °C.

## Conclusions

The aim of this study was to investigate the response of myoblasts to IR laser treatment in order to get further insights into the cellular and molecular mechanisms underlying the effects of laser therapy on muscle tissue described in clinical studies and on animal models. Our results show that laser treatment, with the source and parameters chosen, did not affect cell viability but induced a decrease in cell proliferation and increase in expression of the early differentiation marker MyoD, associated with changes of cell morphology and cytoskeletal architecture leading to the formation of tube-like structures. Taken together, these findings suggest that the exposure to IR laser triggers a differentiation process in myoblasts.

The analysis of differential expression in the proteomic profile of laser treated and untreated cells, which to the best of our knowledge had never been performed before, further confirmed in treated cells a scenario of differentiation process in its early stages. In fact, following laser exposure, numerous proteins known to be involved in cell cycle regulation, cytoskeleton organization and differentiation showed a significant increase or modulation. The fact that IR laser treatment seems to be able to promote myoblast differentiation *in vitro* could in part explain the regenerative and reparative effects attributed to laser therapy when applied to muscle injury in clinics. Very interestingly, the proteomic analysis also revealed the increase of numerous ATP-binding proteins and proteins involved in the regulation of muscle metabolism, as PP1, establishing a connection with the well-known effect of red-IR laser radiation on the activity of cytochrome oxidase and ATP synthesis.[4] Moreover, among the proteins overexpressed in the treated cells there were NLRP 10 and other proteins which regulate the inflammatory response and could contribute to the anti-inflammatory action attributed to laser therapy. Finally, the increase of proteins involved in cell adhesion/migration, angiogenesis and axonogenesis fits with the

possibility to induce by laser treatment mechanisms related to tissue repair processes.

In conclusion, this study reports for the first time a proteomic analysis of IR laser treated myoblasts, thus contributing with original results to shed light on molecular and cellular mechanisms underlying the effect of laser therapy in muscle repair and recovery.

## Acknowledgements

## References

1  A. Gür, M. Karakoç, K. Nas, R. Cevik, J. Saraç and E. Demir, Efficacy of low power laser therapy in fibromyalgia: a single-blind, placebo-controlled trial, *Lasers Med. Sci.*, 2002, **17**(1), 57–61.

2  D. R. dos Santos, R. E. Liebano, C. S. Baldan, I. B. Masson, R. P. Soares and I. J. Esteves, The low-level laser therapy on muscle injury recovery: literature review, *J. Health Sci. Inst.*, 2010, **28**(3), 286–288.

3  E. C. Leal Junior, R. A. Lopes-Martins, P. de Almeida, L. Ramos, V. V. Iversen and J. M. Bjordal, Effect of low-level laser therapy (GaAs 904 nm) in skeletal muscle fatigue and biochemical markers of muscle damage in rats, *Eur. J. Appl. Physiol.*, 2010, **108**(6), 1083–1088.

4  T. I. Karu and S. F. Kolyakov, Exact action spectra for cellular responses relevant to phototherapy, *Photomed. Laser Surg.*, 2005, **23**, 355–361.

5  P. C. Silveira, L. A. Silva, D. B. Fraga, T. P. Freitas, E. L. Streck and R. Pinho, Evaluation of mitochondrial respiratory chain activity in muscle healing by low-level laser therapy, *J. Photochem. Photobiol., B*, 2009, **95**(2), 89–92.

6  E. G. Novoselova, O. V. Glushkova, D. A. Cherenkov, V. M. Chudnovsky and E. E. Fesenko, Effects of low-power laser radiation on mice immunity, *Photodermatol., Photoimmunol. Photomed.*, 2006, **22**(1), 33–38.

7  R. Albertini, A. B. Villaverde, F. Aimbire, M. A. Salgado, J. M. Bjordal, L. P. Alves, E. Munin and M. S. Costa, Anti-inflammatory effects of low-level laser therapy (LLLT) with two different red wavelengths (660 nm and 684 nm) in carrageenan-induced rat paw edema, *J. Photochem. Photobiol., B*, 2007, **89**(1), 50–55.

8  L. Gavish, L. S. Perez, P. Reissman and S. D. Gertz, Irradiation with 780 nm diode laser attenuates inflammatory cytokines but upregulates nitric oxide in lipopolysaccharide-stimulated macrophages: implications for the prevention of aneurysm progression, *Lasers Surg. Med.*, 2008, **40**(5), 371–378.

9  F. Aimbire, F. V. Santos, R. Albertini, H. C. Castro-Faria-Neto, J. Mittmann and C. Pacheco-Soares, Low-level laser therapy decreases levels of lung neutrophils anti-apoptotic

factors by a NF-kappaB dependent mechanism, *Int. Immunopharmacol.*, 2008, **8**(4), 603–605.

10  M. Monici, V. Basile, F. Cialdai, G. Romano, F. Fusi and A. Conti, Irradiation by pulsed Nd:YAG laser induces the production of extracellular matrix molecules by cells of the connective tissues. A tool for tissue repair, *Proc. SPIE*, 2008, **6991**, 69912K.

11  M. M. Marques, A. N. Pereira, N. A. Fujihara, F. N. Nogueira and C. P. Eduardo, Effect of low-power laser irradiation on protein synthesis and ultrastructure of human gingival fibroblasts, *Lasers Surg. Med.*, 2004, **34**(3), 260–265.

12  D. Hawkins and H. Abrahamse, Changes in cell viability of wounded fibroblasts following laser irradiation in broad-spectrum or infrared light, *Laser Chem.*, 2007, **2007**, 71039.

13  M. Monici, F. Cialdai, G. Romano, F. Fusi, M. Egli, S. Pezzatini and L. Morbidelli, An *in vitro* study on tissue repair: impact of unloading on cells involved in the remodelling phase, *Microgravity Sci. Technol.*, 2011, **23**(4), 391–401.

14  J. Feng, Y. Zhang and D. Xing, Low-power laser irradiation (LPLI) promotes VEGF expression and vascular endothelial cell proliferation through the activation of ERK/Sp1 pathway, *Cell. Signalling*, 2012, **24**(6), 1116–1125.

15  S. Y. Yu, J. H. Chiu, S. D. Yang, Y. C. Hsu, W. Y. Lui and C. W. Wu, Biological effect of far-infrared therapy on increasing skin microcirculation in rats, *Photodermatol., Photoimmunol. Photomed.*, 2006, **22**(2), 78–86.

16  R. T. Chow, G. Z. Heller and L. Barnsley, The effect of 300 mW, 830 nm laser on chronic neck pain: a double-blind, randomized, placebo-controlled study, *Pain*, 2006, **124**(1–2), 201–210.

17  J. M. Bjordal, C. Couppé, R. T. Chow, J. Tunér and E. A. Ljunggren, A systematic review of low level laser therapy with location-specific doses for pain from chronic joint disorders, *Aust. J. Physiother.*, 2003, **49**(2), 107–116.

18  W. L. He, C. J. Li, Z. P. Liu, J. F. Sun, Z. A. Hu, X. Yin and S. J. Zou, Efficacy of low-level laser therapy in the management of orthodontic pain: a systematic review and meta-analysis, *Lasers Med. Sci.*, 2012, 22.

19  Y. L. Hsieh, L. W. Chou, P. L. Chang, C. C. Yang, M. J. Kao and C. Z. Hong, Low-level laser therapy alleviates neuropathic pain and promotes function recovery in rats with chronic constriction injury: possible involvements in hypoxia-inducible factor 1α (HIF-1α), *J. Comp. Neurol.*, 2012, **520**(13), 2903–2916.

20  V. Campana, M. Moya, A. Gavotto, L. Spitale, F. Soriano and J. A. Palma, Lasertherapy on arthritis induced by urate crystals, *Photomed. Laser Surg.*, 2004, **22**, 499–503.

21  F. Soriano, V. Campana, M. Moya, A. Gavotto, J. Simes, M. Soriano, R. Soriano, L. Spitale and J. Palma, Photo-modulation of pain and inflammation on microcrystalline arthropathies experimental and clinical results, *Photomed. Laser Surg.*, 2006, **24**, 140–150.

22  M. C. Baez, M. D. Táran, V. Campana, J. C. Simes, P. Pons, J. A. Palma and M. Moya, Marcadores de estrés oxidativo en aterogénesis inducida por hiperfibrinogenemia, *Arch. Cardiol. Mex.*, 2009, **79**, 85–90.

23 C. Reinoso Rubio, J. C. Simes, M. Moya, F. Soriano, J. A. Palma and V. Campana, Inflammatory and oxidative stress markers in experimental crystalopathy are modified by photostimulation, *Photomed. Laser Surg.*, 2009, **27**, 79–84.

24 A. Giuliani, M. Fernandez and M. Farinelli, Very low level laser therapy attenuates edema and pain in experimental models, *Int. J. Tissue React.*, 2004, **26**, 29–37.

25 G. Reddy, Photobiological basis and clinical role of low intensity lasers in biology and medicine, *J. Clin. Laser Med. Surg.*, 2004, **22**, 141–150.

26 F. Tascioglu, O. Armagan, Y. Tabak, I. Corapci and C. Oner, Low power laser in patients with knee osteoarthritis, *Swiss Med. Wkly.*, 2004, **134**, 254–258.

27 L. Brosseau, G. Wells, S. Marchand, I. Gaboury, B. Stokes, M. Morin, L. Casimiro, K. Yonge and P. Tugwell, Randomized controlled trial on low level laser therapy (LLLT) in the treatment of osteoarthritis (OA) on the hand, *Lasers Surg. Med.*, 2005, **36**, 210–219.

28 E. C. Leal Junior, R. A. Lopes-Martins, A. A. Vanin, B. M. Baroni, D. Grosselli, T. De Marchi, V. V. Iversen and J. M. Bjordal, Effect of 830 nm low-level laser therapy applied before high-intensity exercises on skeletal muscle recovery in athletes, *Lasers Med. Sci.*, 2009, **24**(3), 425–431.

29 C. F. Rizzi, J. Z. Mauriz, D. S. Freitas Corrêa, A. J. Moreira, C. G. Zettler, L. I. Filippin, N. P. Marroni and J. González-Gallego, Effects of low-level laser therapy (LLLT) on the nuclear factor (NF)-kappaB signaling pathway in traumatized muscle, *Lasers Surg. Med.*, 2006, **38**(7), 704–713.

30 N. Servetto, D. Cremonezzi, J. C. Simes, M. Moya, F. Soriano, J. A. Palma and V. R. Campana, Evaluation of inflammatory biomarkers associated with oxidative stress and histological assessment of low-level laser therapy in experimental myopathy, *Lasers Surg. Med.*, 2010, **42**(6), 577–583.

31 J. Nakano, H. Kataoka, J. Sakamoto, T. Origuchi, M. Okita and T. Yoshimura, Low-level laser irradiation promotes the recovery of atrophied gastrocnemius skeletal muscle in rats, *Exp. Physiol.*, 2009, **94**(9), 1005–1015.

32 S. Burattini, P. Ferri, M. Battistelli, R. Curci, F. Luchetti and E. Falcieri, C2C12 murine myoblasts as a model of skeletal muscle development: morpho-functional characterization, *Eur. J. Histochem.*, 2004, **48**(3), 223–233.

33 X. Y. Wang and M. A. Rudnicki, Satellite cells, the engines of muscle repair, *Nat. Rev. Mol. Cell Biol.*, 2011, **13**(2), 127–133.

34 T. J. Hawke and D. J. Garry, Myogenic satellite cells: physiology to molecular biology, *J. Appl. Physiol.*, 2001, **91**(2), 534–551.

35 B. H. Penn, D. A. Bergstrom, F. J. Dilworth, E. Bengal and S. J. Tapscott, A MyoD-generated feed-forward circuit temporally patterns gene expression during skeletal muscle differentiation, *Genes Dev.*, 2004, **18**(19), 2348–2353.

36 A. Schmidt and M. N. Hall, Signaling to the actin cytoskeleton, *Annu. Rev. Cell Dev. Biol.*, 1998, **14**, 305–338.

37 G. G. Gundersen, S. Khawaja and J. C. Bulinski, Generation of a Stable, Posttranslationally Modified Microtubule Array Is an Early Event in Myogenic Differentiation, *J. Cell Biol.*, 1989, **109**, 2275–2288.

38 B. Kamińska, L. Kaczmarek and B. Grzelakowska-Sztabert, Inhibitors of polyamine biosynthesis affect the expression of genes encoding cytoskeletal proteins, *FEBS Lett.*, 1992, **304**(2–3), 198–200.

39 G. S. Bennett, S. A. Fellini, Y. Toyama and H. Hollzer, Redistribution of intermediate filament subunits during skeletal myogenesis and maturation *in vitro*, *J. Cell Biol.*, 1979, **82**, 577–584.

40 D. L. Gard and E. Lazarides, The synthesis and distribution of desmin and vimentin during myogenesis *in vitro*, *Cell*, 1980, **19**(1), 263–275.

41 N. S. Tannu, V. K. Rao, R. M. Chaudhary, F. Giorgianni, A. E. Saeed, Y. Gao and R. Raghow, Comparative proteomes of the proliferating C(2)C(12) myoblasts and fully differentiated myotubes reveal the complexity of the skeletal muscle differentiation program, *Mol. Cell. Proteomics*, 2004, **3**(11), 1065–1082.

42 P. F. Van der Ven, G. Schaart, H. J. Croes, P. H. Jap, L. A. Ginsel and F. C. Ramaekers, Titin aggregates associated with intermediate filaments align along stress fiber-like structures during human skeletal muscle cell differentiation, *J. Cell Sci.*, 1993, **106**(Pt 3), 749–759.

43 H. Komati, F. Naro, S. Mebarek, V. De Arcangelis, S. Adamo, M. Lagarde, A. F. Prigent and G. Némoz, Phospholipase D is involved in myogenic differentiation through remodeling of actin cytoskeleton, *Mol. Biol. Cell*, 2005, **16**(3), 1232–1244.

44 A. P. Arrigo, In search of the molecular mechanism by which small stress proteins counteract apoptosis during cellular differentiation, *J. Cell. Biochem.*, 2005, **94**(2), 241–246.

45 O. Geneste, J. M. Copeland and R. Treisman, LIM kinase and Diaphanous cooperate to regulate serum response factor and actin dynamics, *J. Cell Biol.*, 2002, **157**(5), 831–838.

46 G. Pawlak and D. M. Helfman, MEK mediates v-Src-induced disruption of the actin cytoskeleton *via* inactivation of the Rho-ROCK-LIM kinase pathway, *J. Biol. Chem.*, 2002, **277**(30), 26927–26933.

47 A. Keller, J. Peltzer, G. Carpentier, I. Horváth, J. Oláh, A. Duchesnay, F. Orosz and J. Ovádi, Interactions of enolase isoforms with tubulin and microtubules during myogenesis, *Biochim. Biophys. Acta*, 2007, **1770**(6), 919–926.

48 F. Magherini, P. M. Abruzzo, L. Puglia, L. Bini, T. Gamberi, F. Esposito, A. Veicsteinas, M. Marini, C. Fiorillo, M. Gulisano and A. Modesti, Proteomic analysis and protein carbonylation profile in trained and untrained rat muscles, *J. Proteomics*, 2012, **75**(3), 978–992.

49 Y. Wang, M. Hasegawa, R. Imamura, T. Kinoshita, C. Kondo, K. Konaka and T. Suda, PYNOD, a novel Apaf-1/CED4-like protein is an inhibitor of ASC and caspase-1, *Int. Immunol.*, 2004, **16**(6), 777–786.

50 R. Imamura, Y. Wang, T. Kinoshita, M. Suzuki, T. Noda, J. Sagara, S. Taniguchi, H. Okamoto and T. Suda, Anti-inflammatory activity of PYNOD and its mechanism in humans and mice, *J. Immunol.*, 2010, **184**(10), 5874–5884.

51 Y. Liu, H. Yu, S. K. Deaton and B. G. Szaro, Heterogeneous nuclear ribonucleoprotein K, an RNA-binding protein, is

required for optic axon regeneration in *Xenopus laevis*, *J. Neurosci.*, 2012, **32**(10), 3563–3574.

52 I. F. Mohammed, N. Al-Mustawfi and L. N. Kaka, Promotion of regenerative processes in injured peripheral nerve induced by low-level laser therapy, *Photomed. Laser Surg.*, 2007, **25**(2), 107–111.

53 K. Bomsztyk, O. Denisenk and J. Ostrowski, hnRNP K: one protein multiple processes, *Bioessays*, 2004, **26**(6), 629–638.

54 F. T. Liu, R. J. Patterson and J. L. Wang, Intracellular functions of galectins, *Biochim. Biophys. Acta*, 2002, **1572**(2–3), 263–273.

55 J. Ochieng, V. Furtak and P. Lukyanov, Extracellular functions of galectin-3, *Glycoconjugate J.*, 2002, **19**(7–9), 527–535.

56 H. Ceulemans and M. Bollen, Functional diversity of protein phosphatase-1, a cellular economizer and reset button, *Physiol. Rev.*, 2004, **84**, 1–39.

57 N. V. Oleinik, N. I. Krupenko and S. A. Krupenko, ALDH1L1 inhibits cell motility *via* dephosphorylation of cofilin by PP1 and PP2A, *Oncogene*, 2010, **29**(47), 6233–6244.

58 N. C. Kwiek, D. F. Thacker, M. B. Datto, H. B. Megosh and T. A. Haystead, PITK, a PP1 targeting subunit that modulates the phosphorylation of the transcriptional regulator hnRNP K, *Cell. Signalling*, 2006, **18**(10), 1769–1778.

59 C. Cid, L. Garcia-Bonilla, E. Camafeita, J. Burda, M. Salinas and A. Alcazar, Proteomic characterization of protein phosphatase 1 complexes in ischemia-reperfusion and ischemic tolerance, *Proteomics*, 2007, **7**(17), 3207–3218.

60 W. Xu, X. Yuan, Y. J. Jung, Y. Yang, A. Basso, N. Rosen, E. J. Chung, J. Trepel and L. Neckers, The heat shock protein 90 inhibitor geldanamycin and the ErbB inhibitor ZD1839 promote rapid PP1 phosphatase-dependent inactivation of AKT in ErbB2 overexpressing breast cancer cells, *Cancer Res.*, 2003, **63**(22), 7777–7784.

61 J. Qian, E. Vafiadaki, S. M. Florea, V. P. Singh, W. Song, C. K. Lam, Y. Wang, Q. Yuan, T. J. Pritchard, W. Cai, K. Haghighi, P. Rodriguez, H. S. Wang, D. Sanoudou, G. C. Fan and E. G. Kranias, Small heat shock protein 20 interacts with protein phosphatase-1 and enhances sarcoplasmic reticulum calcium cycling, *Circ. Res.*, 2011, **108**(12), 1429–1438.

62 A. Hochwagen, W. H. Tham, G. A. Brar and A. Amon, The FK506 binding protein Fpr3 counteracts protein phosphatase 1 to maintain meiotic recombination checkpoint activity, *Cell*, 2005, **122**(6), 861–873.

63 T. Oguri, A. Inoko, H. Shima, I. Izawa, N. Arimura, T. Yamaguchi, N. Inagaki, K. Kaibuchi, K. Kikuchi and M. Inagaki, Vimentin-Ser82 as a memory phosphorylation site in astrocytes, *Genes Cells*, 2006, **11**(5), 531–540.

64 H. Inada, H. Togashi, Y. Nakamura, K. Kaibuchi, K. Nagata and M. Inagaki, Balance between activities of Rho kinase and type 1 protein phosphatase modulates turnover of phosphorylation and dynamics of desmin/vimentin filaments, *J. Biol. Chem.*, 1999, **274**(49), 34932–34939.

65 C. C. King, K. Bouic and T. Friedmann, A fractionation method to identify quantitative changes in protein expression mediated by IGF-1 on the proteome of murine C2C12 myoblasts, *Proteome Sci.*, 2009, **7**, 28.

66 N. V. Oleinik, N. I. Krupenko and S. A. Krupenko, ALDH1L1 inhibits cell motility *via* dephosphorylation of cofilin by PP1 and PP2A, *Oncogene*, 2010, **29**(47), 6233–6244.

67 S. J. Kim, K. Y. Kim, S. J. Tapscott, T. S. Winokur, K. Park, H. Fujiki, H. Weintraub and A. B. Roberts, Inhibition of protein phosphatases blocks myogenesis by first altering MyoD binding activity, *J. Biol. Chem.*, 1992, **267**(21), 15140–15145.

68 L. Ragolia, Q. Zuo and N. Begum, Inhibition of myogenesis by depletion of the glycogen-associated regulatory subunit of protein phosphatase-1 in rat skeletal muscle cells, *J. Biol. Chem.*, 2000, **275**(34), 26102–26108.

69 J. St-Amand, K. Okamura, K. Matsumoto, S. Shimizu and Y. Sogawa, Characterization of control and immobilized skeletal muscle: an overview from genetic engineering, *FASEB J.*, 2001, **15**(3), 684–692.

70 M. Srinivasan and N. Begum, Regulation of protein phosphatase 1 and 2A activities by insulin during myogenesis in rat skeletal muscle cells in culture, *J. Biol. Chem.*, 1994, **269**(17), 12514–12520.

71 S. Benedicenti, I. M. Pepe, F. Angiero and A. Benedicenti, Intracellular ATP level increases in lymphocytes irradiated with infrared laser light of wavelength 904 nm, *Photomed. Laser Surg.*, 2008, **26**(5), 451–453.

72 T. J. Cheng, Y. L. Lin, A. S. Chiang and Y. K. Lai, Association of protein phosphatase 2A with its substrate vimentin intermediate filaments in 9L rat brain tumor cells, *J. Cell. Biochem.*, 2000, **79**(1), 126–138.

73 S. Mochida and T. Hunt, Protein phosphatases their regulation in the control of mitosis, *EMBO Rep.*, 2012, **13**(3), 197–203.

74 A. Caselli, M. L. Taddei, G. Manao, G. Camici and G. Ramponi, Tyrosine-phosphorylated caveolin is a physiological substrate of the low M(r) protein-tyrosine phosphatase, *J. Biol. Chem.*, 2001, **276**(22), 18849–18854.

75 A. Caselli, R. Marzocchini, G. Camici, G. Manao, G. Moneti, G. Pieraccini and G. Ramponi, The inactivation mechanism of low molecular weight phosphotyrosine-protein phosphatase by H$_2$O$_2$, *J. Biol. Chem.*, 1998, **273**(49), 32554–32560.

76 W. J. Hendriks, A. Elson, S. Harroch, R. Pulido, A. Stoker and J. den Hertog, Protein tyrosine phosphatases in health and disease, *FEBS J.*, 2013, **280**(2), 708–730.

77 F. Magherini, C. Tani, T. Gamberi, A. Caselli, L. Bianchi, L. Bini and A. Modesti, Protein expression profiles in *Saccharomyces cerevisiae* during apoptosis induced by H$_2$O$_2$, *Proteomics*, 2007, **7**(9), 1434–1445.

78 G. Candiano, M. Brusch, L. Musante, L. Santucci, G. M. Ghiggeri, B. Carnemolla, P. Orecchia, L. Zardi and P. G. Rigetti, Blue Silver: A very sensitive colloidal Coomassie G-250 staining for proteome analysis, *Electrophoresis*, 2004, **25**, 1327–1333.

79 A. Shevchenko, M. Wilm, O. Vorm and M. Mann, Mass spectrometric sequencing of proteins silver-stained polyacrylamide gels, *Anal. Chem.*, 1996, **68**(5), 850–858.

80 C. Boccardi, A. Cecchettini, A. Caselli, G. Camici, M. Evangelista, A. Mercatanti, G. Rainaldi and L. Citti,

A proteomic approach to the investigation of early events involved in vascular smooth muscle cell activation, *Cell. Tissue Res.*, 2007, **328**(1), 185–195.

81 W. Huang, B. T. Sherman and R. A. Lempicki, Systematic and integrative analysis of large gene lists using DAVID bioinformatics resources, *Nat. Protoc.*, 2009, **4**, 44–57.

82 K. M. Walton and J. E. Dixon, Protein tyrosine phosphatases, *Annu. Rev. Biochem.*, 1993, **62**, 101–120.

83 A. Caselli, G. Camici, G. Manao, G. Moneti, L. Pazzagli, G. Cappugi and G. Ramponi, Nitric oxide causes inactivation of the low molecular weight phosphotyrosine protein phosphatise, *J. Biol. Chem.*, 1994, **269**(40), 24878–24882.

84 J. Knapp, P. Boknìk, S. Huke, I. Gombosovà, B. Linck, H. Lüss, F. U. Müller, T. Müller, P. Nacke, W. Schmitz, U. Vahlensieck and J. Neumann, Contractility and Inhibition of Protein Phosphatases by Cantharidin, *Gen. Pharmacol.*, 1998, **31**(5), 729–733.

85 H. U. Bergmeyer, *Methods of Enzymatic Analysis*, Academic Press, New York, 2nd edn 1974, vol. 1, pp. 509–510.

86 H. U. Bergmeyer, *in Methods of Enzymatic Analysis*, Academic Press, New York, 2nd edn 1974, vol. 1, p. 449.

87 H. U. Bergmeyer, *in Methods of Enzymatic Analysis*, Academic Press, New York, 1974, vol. 1, p. 481.